

# Pitting Corrosion Behaviour of Boron Added Modified 9Cr–1Mo Steel: Combined Effects of Alkali and Chloride Ions

Namrata Upadhyay · M. G. Pujar · C. R. Das · Nanda Gopal Krishna ·  
C. Mallika · U. Kamachi Mudali

Received: 14 March 2014 / Accepted: 15 July 2014 / Published online: 15 October 2014  
© The Indian Institute of Metals - IIM 2014

**Abstract** Pitting corrosion behaviour of modified 9Cr–1Mo ferritic steel containing 100 ppm of boron was studied in deaerated 0.1, 0.2 and 0.5 M sodium hydroxide solutions containing 0.1, 0.2 and 0.5 M sodium chloride. The chemical compositions of the passive film developed at applied potentials were studied using XPS.  $E_{\text{pit}}$  values decreased with increase in chloride concentrations for the given concentration of alkali. The effect (of  $\text{Cl}^-$ ) was less pronounced in higher alkali concentrations. Pit diameters were observed to be significantly higher in 0.1 M sodium hydroxide containing 0.1 M sodium chloride; with increase in alkali concentration pit diameters were found to be restricted to lower values even at higher chloride concentrations. Energy dispersive spectroscopic (EDS) studies showed that pits had nucleated at  $\text{Al}_2\text{O}_3$  inclusions/matrix interface. XPS analysis revealed the presence of  $\text{Fe}_3\text{O}_4$ ,  $\text{Fe}(\text{OH})_3$  at lower potentials (150 and 209 mV(SCE)) whereas  $\text{Fe}_2\text{O}_3$ ,  $\text{Fe}(\text{OH})_3$  and  $\text{FeO}_2^{2-}$  at higher potentials (400 and 650 mV(SCE)).

**Keywords** 9Cr–1Mo steel · Pitting corrosion · Alkali · Chloride · XPS analysis · Passive film

## 1 Introduction

Ferritic steels are widely used in the power generating industries, chemical processing and petroleum processing industries because of their toughness and high strength at elevated temperatures. Among the chromium–molybdenum series of ferritic steels, 9Cr–1Mo steel in normalized and tempered (N&T) condition has been extensively used in the power generation industries due to its favourable mechanical properties, high temperature strength and corrosion resistance [1]. However, long time exposure of these steels at high temperature or excessive localized heating can result in microstructural changes leading to degradation of mechanical and corrosion properties. In order to increase the high temperature corrosion and oxidation resistance as well as creep properties, these steels are modified by adding carbide forming elements like V, Nb, Ti etc. [2]. The new steels with these additions are known as modified 9Cr–1Mo steels. Modified 9Cr–1Mo ferritic steel is used as a structural material for the steam generator of prototype fast breeder reactor (PFBR) under construction in Kalpakkam [3, 4]. About 100 ppm boron is added to these steels to increase their hardenability as well as creep strength. Since boron has a low solubility in ferrite, it gets incorporated in  $\text{M}_{23}\text{C}_6$  carbides and decreases the rate at which the carbides coarsen, thus stabilizing the microstructure [5–7]. Since all the components (tube, tube sheet and shell) of steam generator are made of modified 9Cr–1Mo steel, it is also required to be resistant against general and localized corrosion.

So far studies have been carried out on the influence of chloride ion concentration as a function of pH on the corrosion behaviour of austenitic stainless steel in aqueous media [8]. However, no studies have been reported on the effect of chloride ions at high pH on the corrosion

N. Upadhyay · M. G. Pujar (✉) · N. G. Krishna · C. Mallika ·  
U. Kamachi Mudali  
Corrosion Science and Technology Group, Indira Gandhi Centre  
for Atomic Research, Kalpakkam, India  
e-mail: pujar@igcar.gov.in

C. R. Das  
Materials Development and Technology Group, Indira Gandhi  
Centre for Atomic Research, Kalpakkam 603 102, India

behaviour of modified 9Cr–1Mo steel vis-à-vis the formation, composition and stability of passive film. An attempt was made to investigate the pitting corrosion behaviour of modified 9Cr–1Mo–B steel in alkaline medium containing chloride ions. Alkaline environment was chosen to simulate the caustic condition generated in the steam generator due to the accidental leak of feed water containing chloride ions (as impurity) into hot sodium [9]. The aim of this paper is to investigate the thickness, composition and stability of the passive film in alkaline media containing different concentrations of chloride ions for better understanding of the pitting corrosion behaviour of modified 9Cr–1Mo steel.

The pitting corrosion studies were carried out using anodic polarization technique. Chemical composition of the passive films was studied using XPS and the surface morphology of the pits was studied using Scanning electron microscopic (SEM) technique attached with EDS.

## 2 Experimental Procedure

### 2.1 Material and Specimen Preparation

Boron-added modified 9Cr–1Mo steel in normalized and tempered (N&T) condition was used in the present work. Chemical composition of the steel is given in Table 1. The specimens with dimensions  $10 \times 10 \times 5 \text{ mm}^3$  were mounted in Araldite resin along with threaded small brass rods to facilitate electrical contact with the specimen holder. While mounting the specimen, proper care was taken to avoid gap between specimen and the resin in order to prevent crevice corrosion attack during pitting corrosion studies using potentiodynamic anodic polarization technique. These specimens were polished up to fine diamond ( $1 \mu\text{m}$ ), washed with soap solution and dried before immersing in the solution. The specimen holder rod connected with the specimen was covered with Teflon tape and was kept out of the solution. The time period between the surface preparation of the specimen and initiation of the anodic polarization experiment was maintained constant.

### 2.2 Potentiodynamic Anodic Polarization Studies

The potentiodynamic anodic polarization experiments were performed in a five-necked polarization cell provided with a Luggin–Haber probe (to separate the bulk solution from the reference electrode) whose tip was in close proximity with the surface of the working electrode. Two auxiliary electrodes (two platinum foils of same area spot-welded to platinum wires) were placed symmetrically on the opposite sides of the working electrode. A salt-bridge was used in order to establish the contact of the working electrode with the reference electrode. All solutions were prepared using double-distilled water and all the potentials were measured against a saturated calomel electrode (SCE). The solution was deaerated for 1 h before starting the experiment by purging high purity argon gas through it for removing the dissolved oxygen and purging was continued during the experiment to avoid oxygen contamination. The specimen was immersed in the solution 45 min before the start of the experiment in order to observe the stable open circuit potential (OCP). The anodic polarization experiments were started from the potential which was 200 mV active to OCP and continued till the current reached 1 mA to ensure that the specimen underwent a stable pitting corrosion attack. The anodic polarization experiments were performed in 0.1, 0.2 and 0.5 NaOH with and without the addition of 0.1, 0.2 and 0.5 NaCl to them. Solartron SI 1287, Solartron, UK computer controlled electrochemical system was used to conduct all the experiments.

### 2.3 Surface Analysis

#### 2.3.1 Microstructural Studies

After the potentiodynamic anodic polarization experiments, the specimens were cleaned with distilled water to remove any loose corrosion deposits and chemically etched with Villela's reagent to observe the microstructure. The specimens were immersed in the etchant for 20 s, cleaned with distilled water, dried and observed under an optical microscope at a magnification of  $50\times$  to determine the approximate size and distribution of pits. Thirty pits were

**Table 1** Chemical composition of modified 9Cr–1Mo steel (wt%)

Elements	C	Cr	Mo	Si	Mn	V	Nb	S
Alloy B	0.1	8.5	1.04	0.40	0.30	0.23	0.09	0.002
Elements	P	Ni	Al	Ti	N	B	Cu	Fe
Alloy B	0.005	0.002	0.03	0.003	0.0021	0.0100	0.006	Bal.

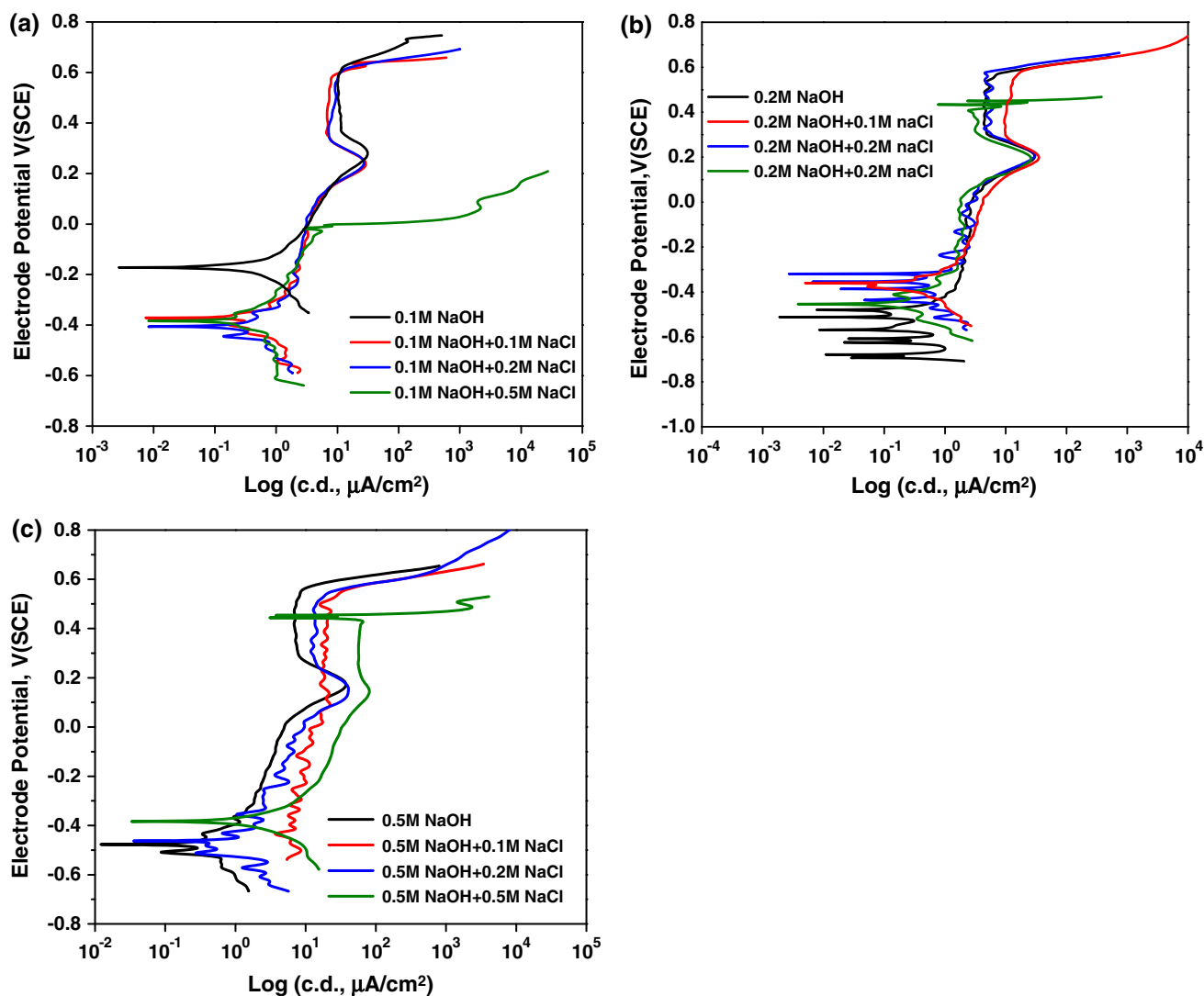


**Fig. 1** Potentiodynamic anodic polarization curves for modified 9Cr-1M-B in **a** 0.1 M NaOH, **b** 0.2 M NaOH and **c** 0.5 M NaOH with and without the addition of 0.1, 0.2 and 0.5 M NaCl

randomly selected at different locations and their diameters were obtained by manual measurements (at least two diameters perpendicular to each other), averaging them and converting them to  $\mu\text{m}$  scale from the magnification used. SEM (CamScan 3200, UK) was used to observe the pit morphology.

### 2.3.2 X-ray Photoelectron Spectroscopic Analysis (XPS)

The specimens were passivated for 1 h in 0.2 M NaOH containing 0.2 M NaCl, at 150, 209, 400 and 650 mV(SCE) potentials which were chosen from the polarization curve. The passivated specimens were rinsed using DD water. The passivated surfaces were analyzed for the chemical composition of the passive film using XPS. The XPS analysis was conducted using SPECS make XPS

system with Al K $\alpha$  source and a PHOIBOS 150 analyzer with a chosen energy resolution for recording survey spectra. The pressure in the analysis chamber was maintained at  $2 \times 10^{-9}$  mbar throughout the measurements. The spectra were collected and analyzed using SPECS Lab 2 data analysis software.

## 3 Results and Discussion

Potentiodynamic anodic polarization curves for the boron added 9Cr-1Mo steel obtained in deaerated 0.1, 0.2 and 0.5 M sodium hydroxide solutions with and without the addition of 0.1, 0.2 and 0.5 M sodium chloride are shown in Fig. 1a–c. Since the alkaline solution was deaerated by purging with ultra-high purity argon gas, water molecules

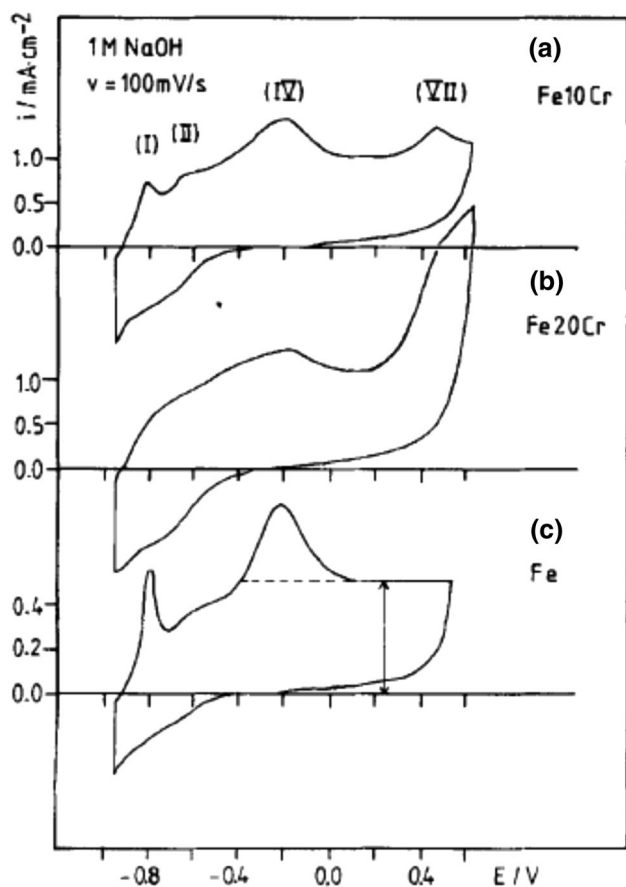
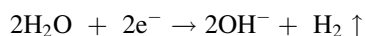


**Fig. 2** Potentiodynamic polarization curves obtained with oxide-free, Ar-sputter-cleaned surfaces of: **a** Fe10Cr, **b** Fe20Cr, **c** pure Fe in 1 M NaOH [10]

present at the metal/solution interface underwent reduction as,



Higher pH of the solution results in the passivation of the specimen, thus, the OCP values were found to be nobler than the primary passivation potentials ( $E_{pp}$ ) commonly observed in the sulphuric acid medium. It was observed that the OCP value became more active in 0.2 and 0.5 M sodium hydroxide solutions ( $\sim -0.5$  V(SCE)) compared to that observed in 0.1 M sodium hydroxide ( $\sim -0.2$  V(SCE)), thus it is apparent that increase in the alkali concentration made the OCP value more active. A distinct peak was noted in the passive region at  $\sim 0.2$  V(SCE) in all the alkali solutions at all concentrations of sodium chloride except in 0.1 M sodium hydroxide containing 0.5 M sodium chloride, where specimen underwent stable pitting at much active potential. In an earlier work [10] on the potentiodynamic anodic polarization studies on the argon-sputter cleaned surface of Fe–10Cr ferritic steel as well as pure iron in deaerated 1 M sodium hydroxide solution, four distinct peaks were observed for Fe–10Cr steel (Fig. 2). These

peaks were identified as Peak (I), Peak (II), Peak (IV) and Peak (VII) at  $-1.041$ ,  $-0.914$ ,  $-0.441$  and  $+0.214$  V(SCE) respectively (converted to SCE scale from the original peak positions on SHE scale for comparison with the present work). The OCP value observed for this steel [10] was more active compared to the one observed for our steel because, (a) complete removal of the originally existing passive film on the argon-sputter cleaned surface, (b) higher alkali concentration (1 M sodium hydroxide) compared to the concentrations of alkali used in the present work, (c) chemical composition difference (the steel specimens used in the present work has molybdenum, niobium and vanadium as well as about 100 ppm of boron, some of these elements enhanced the passive behavior of the steel). Among the above peaks, Peak (I), Peak (II) and Peak (IV) were observed in pure iron too, which indicated that some of the basic corrosion reactions were common to both pure iron as well as Fe–10Cr and alloys with similar compositions. Thus, Peak (I) corresponded to the oxidation of adsorbed hydrogen and Peak (II) corresponded to the anodic dissolution of Fe to form Fe(II) oxide and Peak (IV) to the oxidation of Fe(II) hydroxide to Fe(III) oxide. The Peak (VII) shown in Fig. 2 at  $0.214$  V(SCE) indicated the transpassive dissolution of Cr and the oxidation of Cr(III) to chromate, which was conspicuously absent in the polarization curve of pure iron [10]. In the present work, the peaks corresponding to the dissolution of Cr (Peak (VI) in Fig. 1a–c) were observed at slightly different potentials ( $0.28$ ,  $0.197$  and  $0.172$  V(SCE) in  $0.1$ ,  $0.2$  and  $0.5$  M sodium hydroxide solutions respectively) which could be attributed to the influence of increasing alkali concentrations which lowered OCP values, marginal difference in chemical composition, scan rate and surface preparation, on the dissolution kinetics of Cr. At and above  $-0.441$  V(SCE) Fe(III) overlayer formed in Fe–10Cr steel and a very negligible amount of Fe(II) was left under Fe(III) layer [10]. Chromium content in the passive films of such alloys varied with applied potential and an enrichment of Cr(III) was observed in the inner part whereas the outer part of the passive film was enriched with Fe(III). It was reported that [10] such steels showed a complex passive film with an inner Fe(II)/Cr(III) and an outer Fe(III)/Cr(III) part at potentials more active than  $-0.241$  V(SCE) whereas at potentials more noble than  $-0.241$  V(SCE) a single layered structure with an Fe(III)/Cr(III) formed. At higher potentials, the potential increase affected the Fe(III) containing outer layer which grew linearly with applied potential and time and in the transpassive region kinetics of metal dissolution as well as oxidation of Cr(III) to soluble chromates increased. In the present case too, a film with similar chemical composition is expected to be formed when the electrode is polarized anodically beyond OCP, where passive film richer in Fe(III)/Cr(III) would form preferentially.

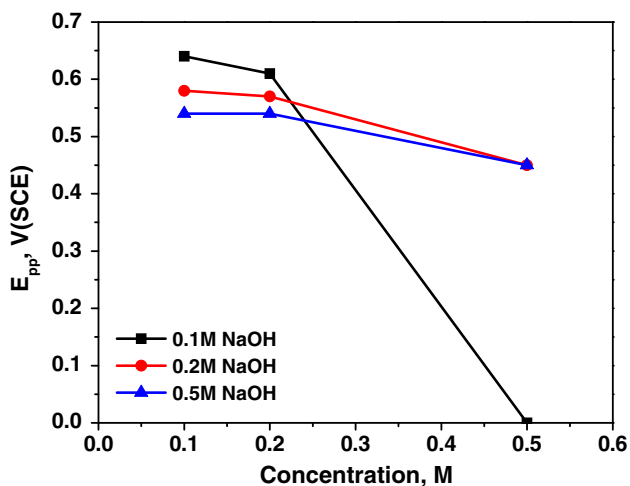
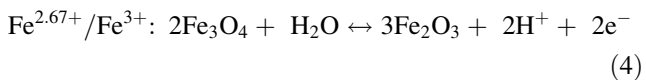
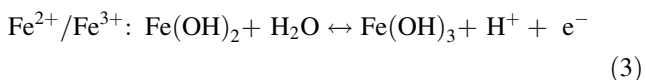
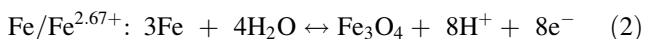
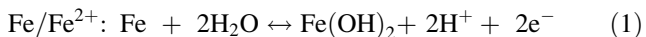


**Fig. 3**  $E_{pit}$  values for modified 9Cr-1Mo-B in different concentrations of alkali solutions in presence of 0.1, 0.2 and 0.5 M NaCl solutions

Pitting potential ( $E_{pit}$ ) was defined as the potential where a monotonic increase in the current was noticed. The plots of  $E_{pit}$  values as a function of chloride ion concentration are shown in Fig. 3. It was observed that except in 0.1 M sodium hydroxide solution where the addition of 0.5 M sodium chloride resulted in the drastic reduction of the  $E_{pit}$  value, the  $E_{pit}$  values in 0.2 and 0.5 M sodium hydroxide solution decreased gradually, decrease being much less compared to that observed in the former.

It has been reported that the stable solid forms of iron at pH ~ 10.5 at 25 °C are metallic iron, ferrous hydroxide [Fe(OH)<sub>2</sub>], magnetite (Fe<sub>3</sub>O<sub>4</sub>), and ferric hydroxide [Fe(OH)<sub>3</sub>](or hematite [Fe<sub>2</sub>O<sub>3</sub>]), depending upon the applied potential [11]. Hydroxides are reported to be more stable solids at ambient temperature [12]. In case of the corrosion of pure iron at pH 10.5 at ambient temperature, the following reactions take place [13],



These compounds are least soluble in weakly alkaline solutions at room temperature and offer protection to the iron surface. Since local acidification is essential feature for pitting corrosion, the burst of protons in a chemical reaction (Eqs. 1–4) could trigger acidic environment destroying this film and consequently the protection

offered by it. Thus, hydrolysis of metal ions (formation of an oxide or hydroxide film) releases protons at the metallic surface and act as a source of acidity for pitting, apart from chloride ions and electrode potential. Some workers have reported increase in  $E_{pit}$  values for pure iron at a constant concentration of 0.1 M sodium chloride in the buffered solutions of 10.5 pH prepared from N<sub>2</sub>B<sub>4</sub>O<sub>7</sub>/NaOH, with increase in the concentrations of borate. However, this increase was attributed to the presence of buffering species which did not allow the pH change in the occluded regions, thereby  $E_{pit}$  values were found to increase [13]. However, in the present work, unbuffered solutions of sodium hydroxide and sodium chloride were used, thus in the absence of the effect of buffering agent, dominating effect of chloride ions and pH change could be observed clearly. At a constant chloride concentration, decrease in  $E_{pit}$  values (which becomes less significant with increase in alkali concentration) was attributed to the formation of soluble species like HFeO<sub>2</sub><sup>-</sup> and FeO<sub>2</sub><sup>-</sup> which will be discussed later. For 0.5 M NaCl solution when the alkali concentration was increased from 0.2 to 0.5 M no change in  $E_{pit}$  was observed, this could be attributed to decrease in local acidification due to increase in pH.

The cumulative probability (CP) F(D) at each D is determined from the set of D values according to the mean rank approximation [14], where D is the pit diameter measured using an optical microscope. According to this method (using D as an example): (1) all the values of D were sorted in an ascending order and (2) then the CP for each value was calculated as n/(N + 1), where n is the position in the sorted list, and N is the total number of entries in the list [15]. The CP plots of pit diameters were prepared at constant concentrations of sodium chloride in different concentrations of sodium hydroxide, Fig. 4a–c. On observing these plots, it was clear that, except in 0.1 M sodium chloride concentration, where the CP plots at different alkali concentrations overlapped to some extent, in the 0.2 and 0.5 M sodium chloride solutions, clearly resolved plots were observed. Pits with larger diameters were observed at a given chloride concentration in the alkaline solution with lower concentration. Pit diameters were found to decrease significantly even in 0.2 and 0.5 M sodium chloride in presence of 0.2 and 0.5 M sodium hydroxide solutions, showing a powerful effect of arresting pit growth due to increased alkali. This could be considered to be a significant observation as the pit diameters were found to be restricted up to a maximum value of 10–12 μm in 0.5 M sodium hydroxide solution containing 0.2 and 0.5 M sodium chloride solutions. Thus, increased alkali concentration did not favour the pit growth by way of increasing pH of the solution existing in the pit bottoms.

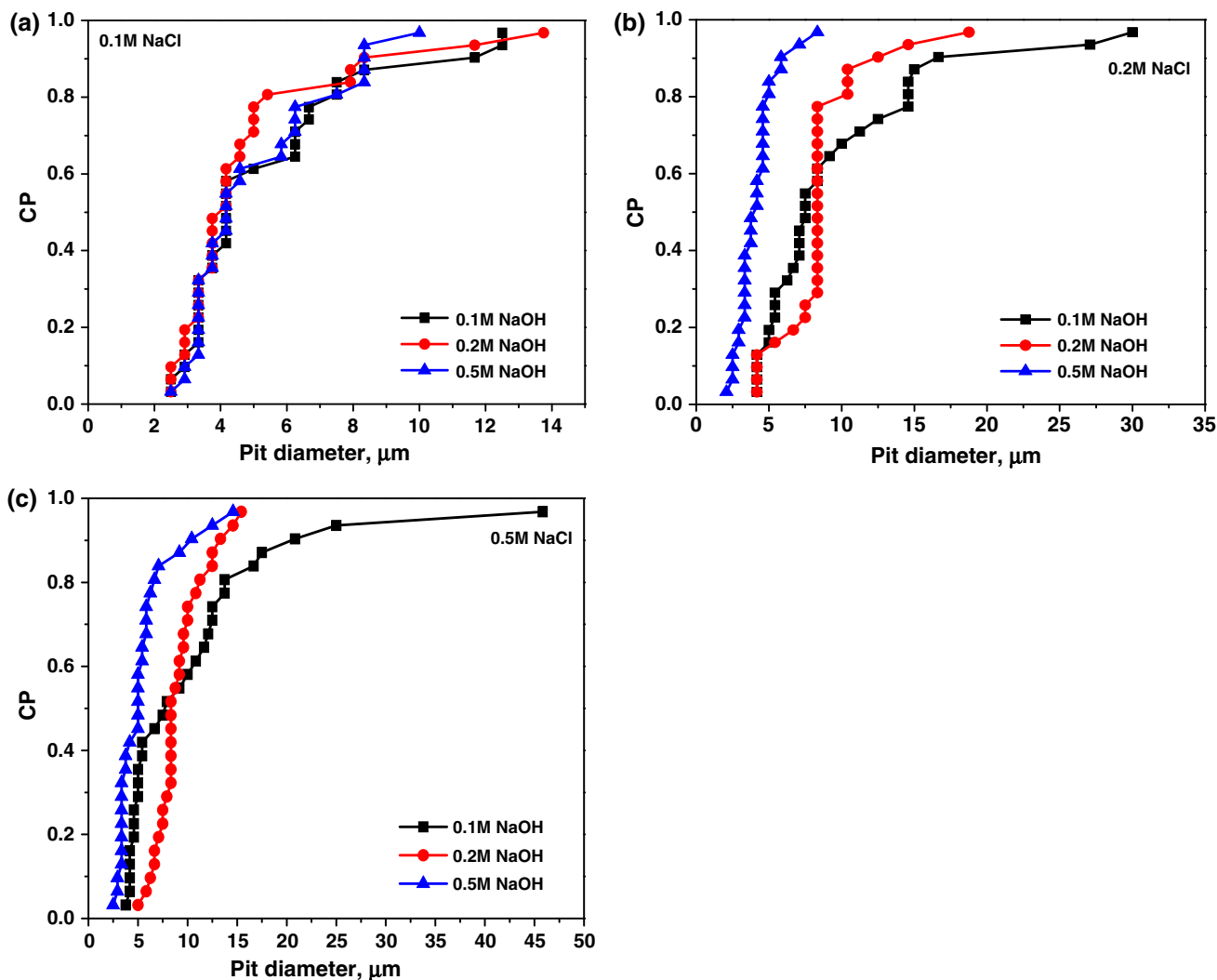


**Fig. 4** CP plots as a function of pit diameter for **a** 0.1 M NaCl, **b** 0.2 M NaCl and **c** 0.5 M NaCl in presence of different concentrations of alkali

The SEM photomicrographs of the pitted specimens are shown in Figs. 5, 6 and 7) which show the morphology of pits as well as pit nucleation sites clearly. Figure 5a, b shows the photomicrographs of specimens pitted in 0.1 M sodium hydroxide solution after the addition of 0.1 and 0.5 M sodium chloride respectively. It was observed that pit size increased significantly with increase in chloride concentration (Fig. 5b). It was observed that pits were nucleated at the boundary of  $M_{23}C_6$  carbide particle/matrix boundaries and grew in the matrix; several such particles are clearly visible inside the grown pit in Fig. 5b. Fivefold increase in the chloride ion concentration resulted in increased pitting corrosion attack as can be seen from the multitude of pits which were observed to be at different stages of their growth. Simultaneous pit initiation at a number of susceptible sites could be the reason for the most active  $E_{pit}$  value in this medium. The smaller pits in Fig. 6a, b were observed in 0.2 M sodium hydroxide

containing 0.2 M sodium chloride solution; the pit diameters were observed to be about 1–2 μm. These were essentially metastable pits at different stages of their growth, where two pits were found to be nucleated around  $M_{23}C_6$  carbide particles (Fig. 6b); the drastic reduction in the pit diameters show the effect of alkali concentration in arresting the pit growth kinetics. Figure 7a, b show the SEM photomicrographs of specimens pitted in 0.5 M sodium hydroxide containing 0.1 M sodium chloride solution. The circular as well as irregularly shaped pits were found to be very shallow, as substructure could be clearly observed inside the pit bottoms. It has been reported that pit nucleation rate was faster during immersion studies because the continuous presence of aggressive electrolytes and a poor protective layer allowed water, chloride ions, and sodium ions to easily reach the surface and nucleate more corrosion pits on the specimen surface. In such environments pits grew faster and then coalesced with each

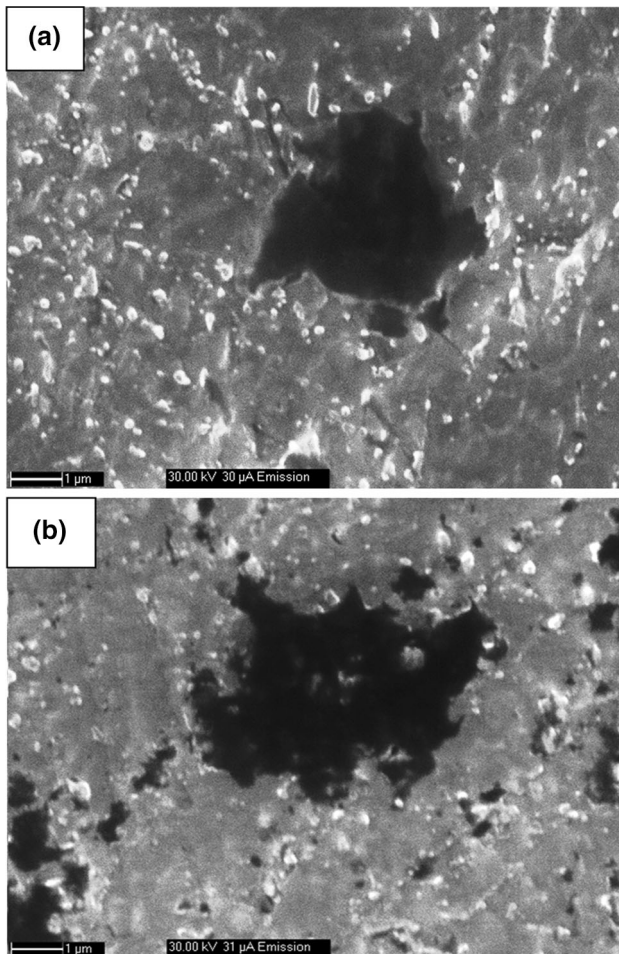


**Fig. 5** SEM photomicrographs of modified 9Cr-1Mo-B pitted specimen in **a** 0.1 M NaOH + 0.1 M NaCl, **b** 0.1 M NaOH + 0.5 M NaCl

other after reaching a certain size. [16] Many such pits were found to coalesce which appeared like uniform corrosion attack on the surface; therefore, it can be said that several such coalesced pits which were shallow in nature, appeared to give a picture as if the specimen surface was suffering from uniform corrosion. Thus, ineffectiveness of chloride ions in causing deep pits could be attributed to the weak passive film developed in the high pH of the solution. Figure 8a shows a pit which was nucleated at the  $\text{Al}_2\text{O}_3$  inclusion/matrix interface; Fig. 8b shows the EDS confirming the presence of  $\text{Al}_2\text{O}_3$  inclusion, the elemental analysis of the same is given in Table 2. Thus, inclusions provided additional sites for pit initiation apart from  $\text{M}_{23}\text{C}_6$  carbides.

### 3.1 XPS Analysis

The XPS analysis was carried out on the potentiostatically passivated specimens at a few selected potentials. The

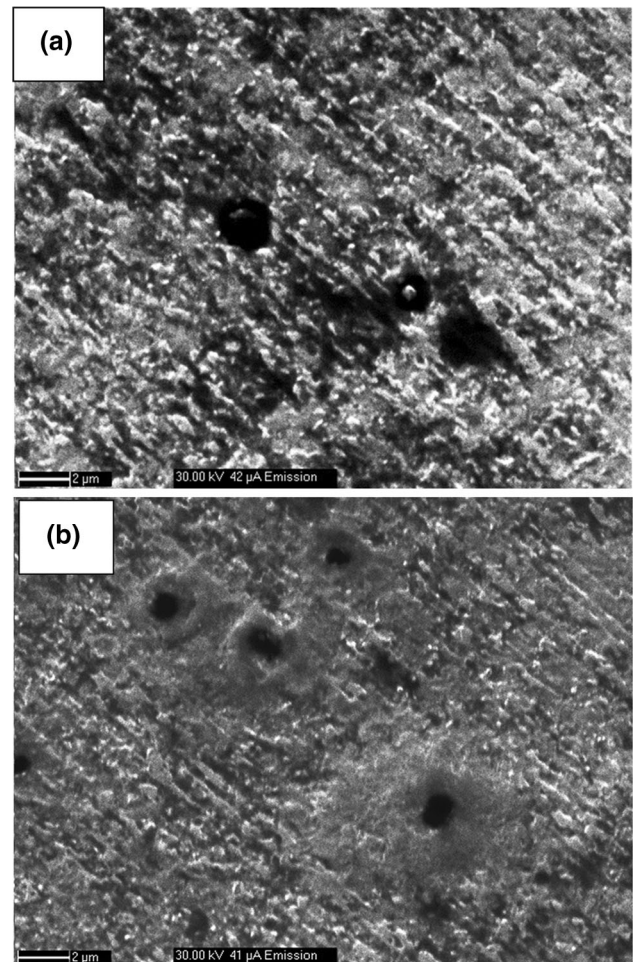


**Fig. 6** SEM photomicrographs of modified 9Cr-1Mo-B pitted specimen in 0.2 M NaOH + 0.2 M NaCl (**a**, **b**)

specimens were passivated in 0.2 M sodium hydroxide containing 0.2 M sodium chloride to avoid extreme concentrations of both alkali as well as chloride ions. The selected passivation potentials were 0.15, 0.209, 0.4 and 0.65 V(SCE) in order to know the state and composition of the passive film before the onset of dissolution at Peak (VI), at the Peak (VI), after the Peak (VI) (i.e. 209 mV(SCE)) and into the pitting region respectively. Instantaneous passivation at these potentials (by directly applying the necessary passive potentials potentiostatically) was avoided, so as to observe the cumulative effect of anodic polarization on passive film through OCP till the selected potential was reached. Analysis of the four specimens showed the presence of Fe, Cr and O as the major elements of the passive film; however, presence of Mo could not be detected on any of these specimens. Intensity of Mo started to increase only after sputtering. The passive films on all the specimens could be almost completely removed after sputtering for 2.5 min. The high resolution scans of Fe and Cr for the 2p core level regions and of O 1s

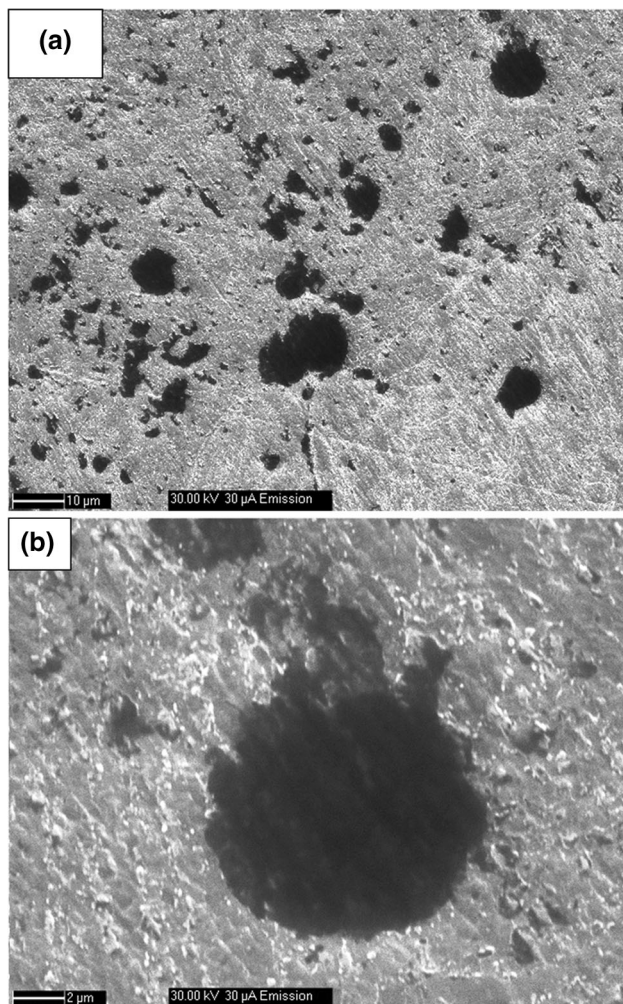


**Fig. 7** SEM photomicrographs of modified 9Cr-1Mo-B pitted specimen in 0.5 M NaOH + 0.1 M NaCl solutions (a, b)

were acquired at every stage of sputtering. This showed that Fe and Cr existed mainly as oxides on the surface and their concentrations decreased after sputtering with respect to their metallic counterparts. A rigorous de-convolution method was followed to find out the actual oxidation states of Fe and Cr as well as their concentrations. A complete multiplet splitting phenomenon was used for this purpose for accuracy.

The Fe 2p ionization was de-convoluted into two different contributions, Fe oxide and Fe metal as shown in Fig. 9a–d. These contributions were assigned to the presence of Fe(0) (binding Energy,  $E_b = 707.0$  eV) and a group of Fe oxides such as  $Fe^{2+}$  oxide ( $E_b = 709.0$ – $709.5$  eV),  $Fe^{3+}$  oxide form ( $E_b = 710.5$ – $711.5$  eV) and also the hydroxide form ( $E_b = 712.0$ – $712.5$  eV) [17]. In all Fe 2p spectra, the dominant peak was associated with the presence of  $Fe^{3+}$  species, mainly in oxides and hydroxides. It has been reported that the determination of  $Fe^{3+}$  contribution among  $Fe_2O_3$  and  $Fe_3O_4$  oxides is a difficult task. In  $Fe_3O_4$  33.3 %

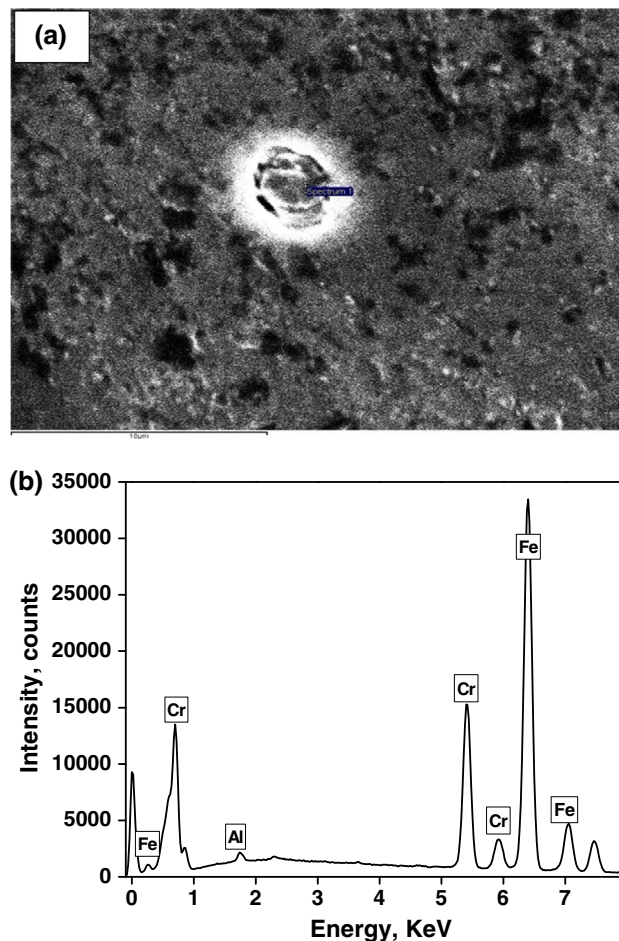


**Fig. 8** SEM photomicrograph of modified 9Cr-1Mo-B pitted specimen in a 0.1 M NaOH + 0.1M NaCl showing pit nucleation at  $Al_2O_3$ /matrix interface, b EDS spectrum showing the presence of the Al peak

of iron is in the  $Fe^{2+}$  state whereas 66.7 % is in the  $Fe^{3+}$  state. It was reported that the  $Fe^{3+} 2P_{3/2}$  peak for  $Fe_3O_4$  was observed at 711.4 eV whereas  $Fe^{2+} 2P_{3/2}$  peak was observed at 709.0 eV in the ratio of 2:1 while O 1s was observed at 530.2 eV [18]. The presence of  $Fe_3O_4$  could be confirmed by analyzing the ratio of the areas of peaks of  $Fe^{3+}$  and  $Fe^{2+}$  respectively, which was 2:1. Since the ratio of peaks was found to be 2:1 in the spectra of steel passivated at a potential of 150 and 209 mV(SCE) but not for the spectra of specimens passivated at 400 and 650 mV(SCE), it was concluded that the passive film on the specimens passivated at 209 and 150 mV(SCE) consisted of  $Fe_3O_4$  whereas it existed as  $Fe_2O_3$  for the specimens passivated at 400 and 650 mV(SCE) respectively. The presence of  $Fe^{2+}$  ions at 150 and 209 mV suggested the initial formation of  $Fe(OH)_2$  (B.E of  $709.6 \pm 0.2$  eV) which was further oxidized to magnetite as per the following chemical reaction [19].

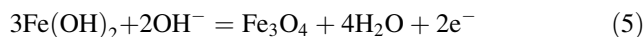




**Table 2** EDS data for the alumina inclusion observed in the pitted specimen

Element	Wt%	Atom%
Al	37.99	55.69
Cr	7.24	5.51
Fe	54.77	38.80

Fe<sup>3+</sup> peak observed at 712.3 ± 0.2 eV was assigned to Fe(OH)<sub>3</sub> [20]. Similar peaks were observed in all the spectra (Fig. 9a–d) indicating the presence of Fe(OH)<sub>3</sub> in the passive film at all the above potentials. Fe(OH)<sub>3</sub> can either form directly as Fe + 3OH<sup>-</sup> = Fe(OH)<sub>3</sub> + 3e<sup>-</sup> or from Fe(OH)<sub>2</sub> and water molecules as shown in Eq. (3).

**Table 3** XPS analysis of ratio of peak areas of Fe<sup>3+</sup>/Fe<sup>2+</sup>

Electrode Potential, V(SCE)	Total peak area of Fe <sup>3+</sup> (%)	Total peak area of Fe <sup>2+</sup> (%)	Fe <sup>3+</sup> /Fe <sup>2+</sup>
0.150	56.087	20.298	2.8:1
0.209	57.532	16.9768	3.4:1
0.400	53.243	33.453	1.6:1
0.650	45.766	34.571	1.3:1

The Fe<sup>2+</sup> peaks were clearly observed in the XPS plots obtained at 0.4 and 0.65 V(SCE). The Fe<sup>2+</sup> ions form Fe(OH)<sub>2</sub> which on electrooxidation transforms to more stable species like HFeO<sub>2</sub><sup>-</sup> and FeO<sub>2</sub><sup>2-</sup>. These species being water soluble weaken the passive film, where uniform dissolution becomes predominant rather than pitting

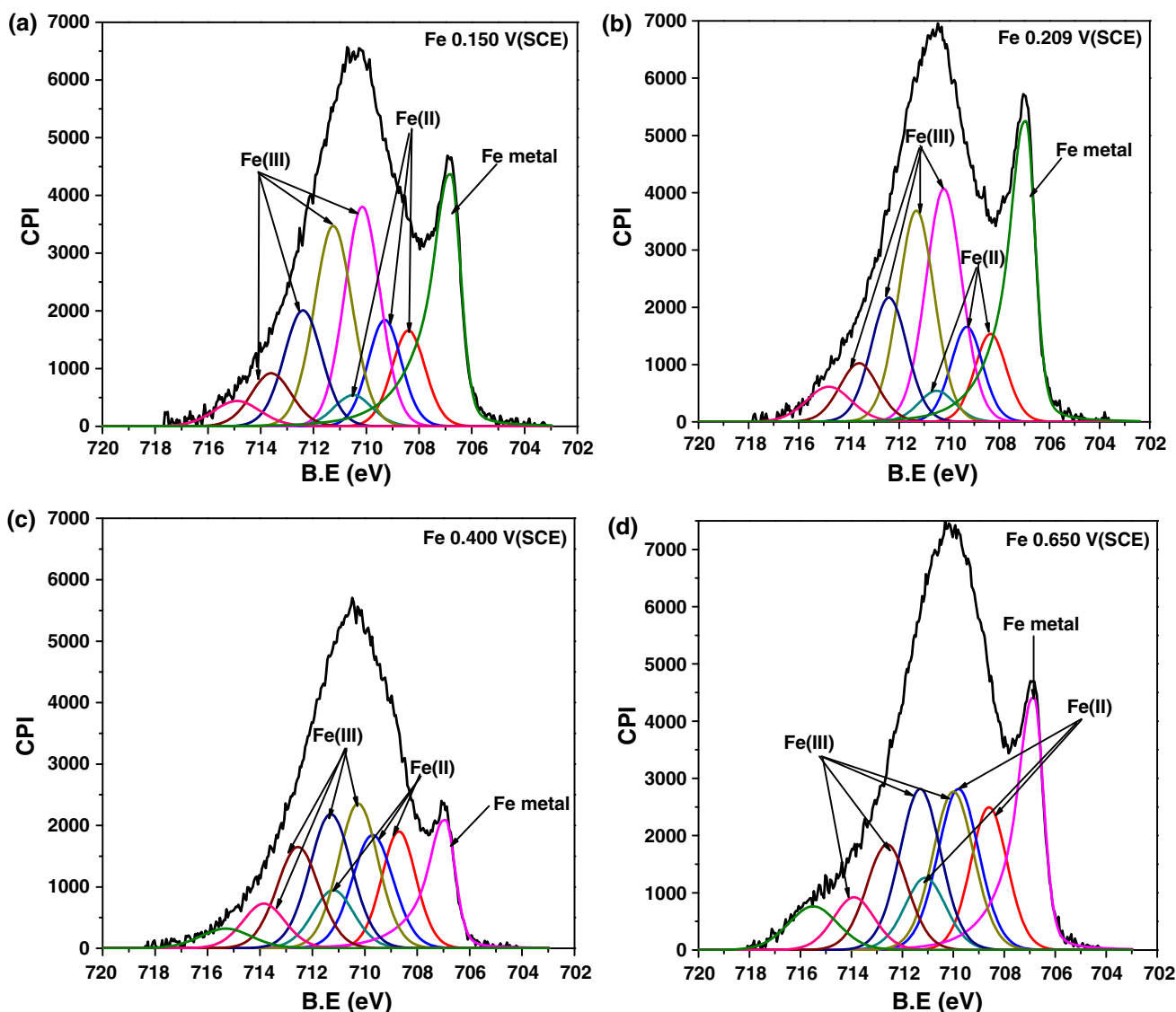
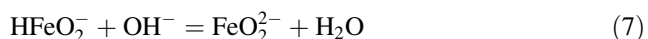
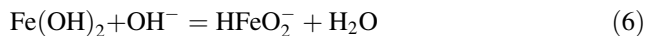


**Fig. 9** The XPS spectra showing iron peaks for potentiostatically polarized specimens at a 150 mV, b 209 mV, c 400 mV and d 650 mV(SCE) potentials

**Table 4** XPS analysis of peaks of Fe(2p) compounds

Compound	Species	Main peak (eV)
Fe(0)/metal	Fe(0)	706.8
Fe <sub>3</sub> O <sub>4</sub> (magnetite)	Fe <sup>2+</sup> 2p <sub>3/2</sub>	709.0
	Fe <sup>3+</sup> 2p <sub>3/2</sub>	711.4
α-Fe <sub>2</sub> O <sub>3</sub> (haematite)	Fe <sup>3+</sup> 2p <sub>3/2</sub>	710.8
Iron(III) hydroxide.	Fe <sup>3+</sup> 2p <sub>3/2</sub>	712.1

corrosion particularly at higher pH as per the following reactions,



The total peak area ratio of Fe<sup>3+</sup> and Fe<sup>2+</sup> was calculated for the specimens passivated at different potentials. It was found that this ratio of Fe<sup>3+</sup>/Fe<sup>2+</sup> initially increased when the potential was increased from 150 to 209 mV(SCE); however, the ratio started to decrease with increase in the potential from 400 to 650 mV(SCE). The ratio of Fe<sup>3+</sup>/Fe<sup>2+</sup> at different potential is given in Table 3. Thus, at low potential Fe<sup>2+</sup> exists in low proportion and its proportion increases at higher passive potentials. This could be attributed to the formation of more stable species of Fe<sup>2+</sup> at higher potential such as Fe<sup>3+</sup> and HFeO<sub>2</sub><sup>-</sup> and FeO<sub>2</sub><sup>2-</sup>. The decrease in the ratio of Fe<sup>3+</sup>/Fe<sup>2+</sup> could be attributed to either (i) transpassive dissolution in alkaline solutions without

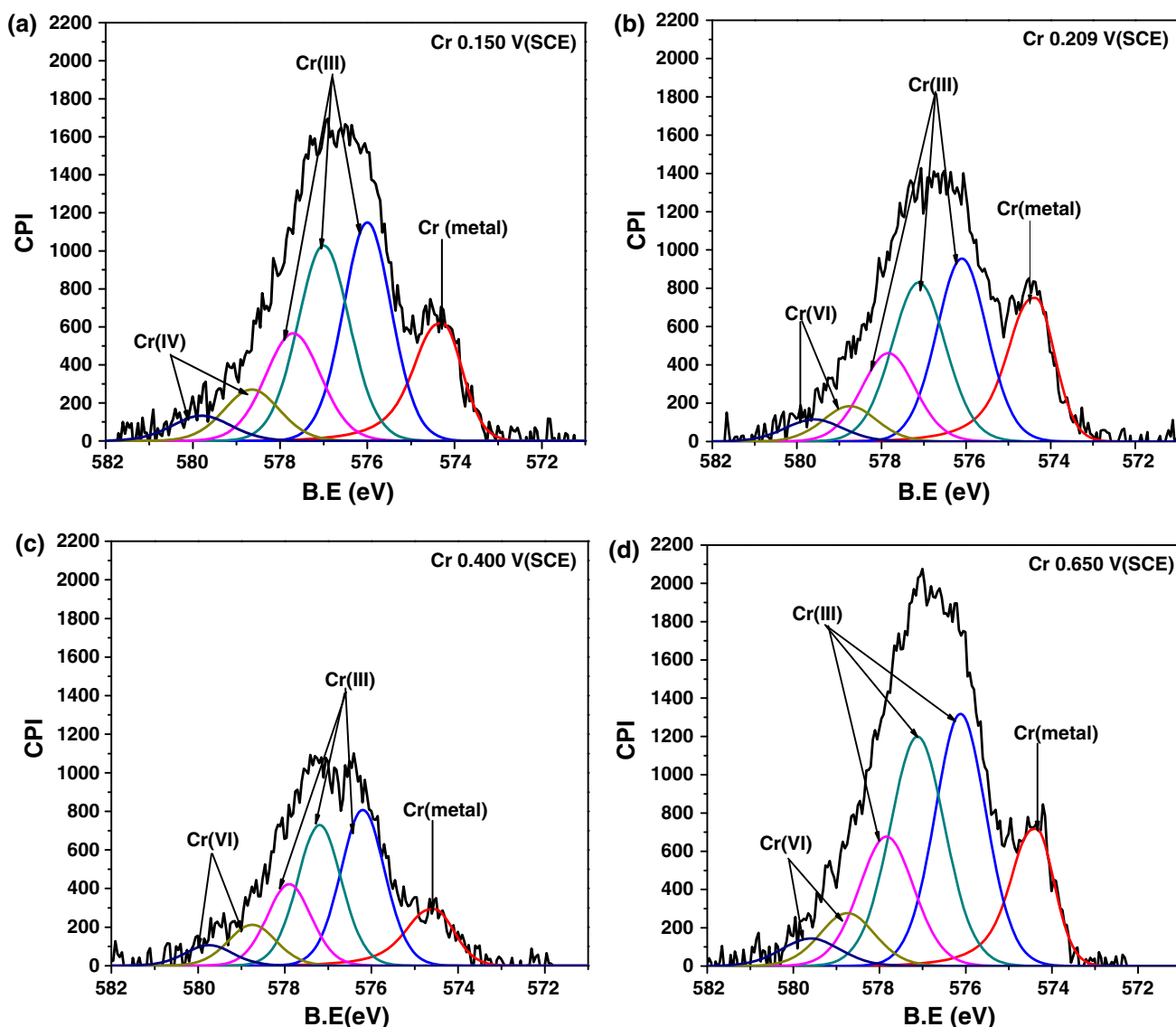


**Fig. 10** The XPS spectra showing chromium peaks for potentiostatically polarized specimens at **a** 150 mV, **b** 209 mV, **c** 400 mV and **d** 650 mV(SCE) potentials

**Table 5** X-ray photoelectron spectroscopic studies of chromium compounds

State/type of compound	Binding energy determined from this work (eV)	Average binding energy obtained from literature (eV)
Cr(O)/metal	574.36	574.2
Cr(III)/Cr <sub>2</sub> O <sub>3</sub>	576.12	576.5
Cr(III)/Cr(OH) <sub>3</sub>	577.12	577.2
Cr(III)/CrCl <sub>3</sub>	577.84	577.6
Cr(VI)/CrO <sub>3</sub>	578.75	579.2
Cr(VI)/(Cr <sub>2</sub> O <sub>7</sub> ) <sup>2-</sup>	579.60	579.6

chloride ions, or (ii) pitting corrosion. Thus, Fe exists in the passive film in the form of Fe<sub>2</sub>O<sub>3</sub>, Fe(OH)<sub>3</sub> and FeO<sub>2</sub><sup>2-</sup> on the specimens passivated at 400 and 650 mV(SCE), while it exists as Fe<sub>3</sub>O<sub>4</sub> (magnetite) and Fe(OH)<sub>3</sub> at 150 and

209 mV(SCE) respectively. Pourbaix diagram of iron at high pH shows initial formation of Fe<sub>3</sub>O<sub>4</sub> followed by the formation of Fe<sub>2</sub>O<sub>3</sub> with increase in potential. Usually three different types of iron oxides are identified viz. FeO, Fe<sub>3</sub>O<sub>4</sub> and Fe(III) where Fe(III) represents both Fe<sub>2</sub>O<sub>3</sub> and FeOOH [21]. The passive film is generally considered to consist of an inner chromium oxide rich film and an outer hydroxide film [22], which is explained by iron dissolving and chromium getting enriched and oxidised [23]. A possible explanation to iron on top of chromium hydroxide [24] is that when the local surface concentration of iron ions increases, iron hydroxides precipitate and form a hydroxide layer on top of chromium hydroxide. Thus, during transpassive dissolution or pitting corrosion, the possibility of FeOOH loss would decrease the Fe(III)/Fe(II) ratio automatically. The B.E of Fe 2p<sub>3/2</sub> compounds obtained from literature are given in Table 4.

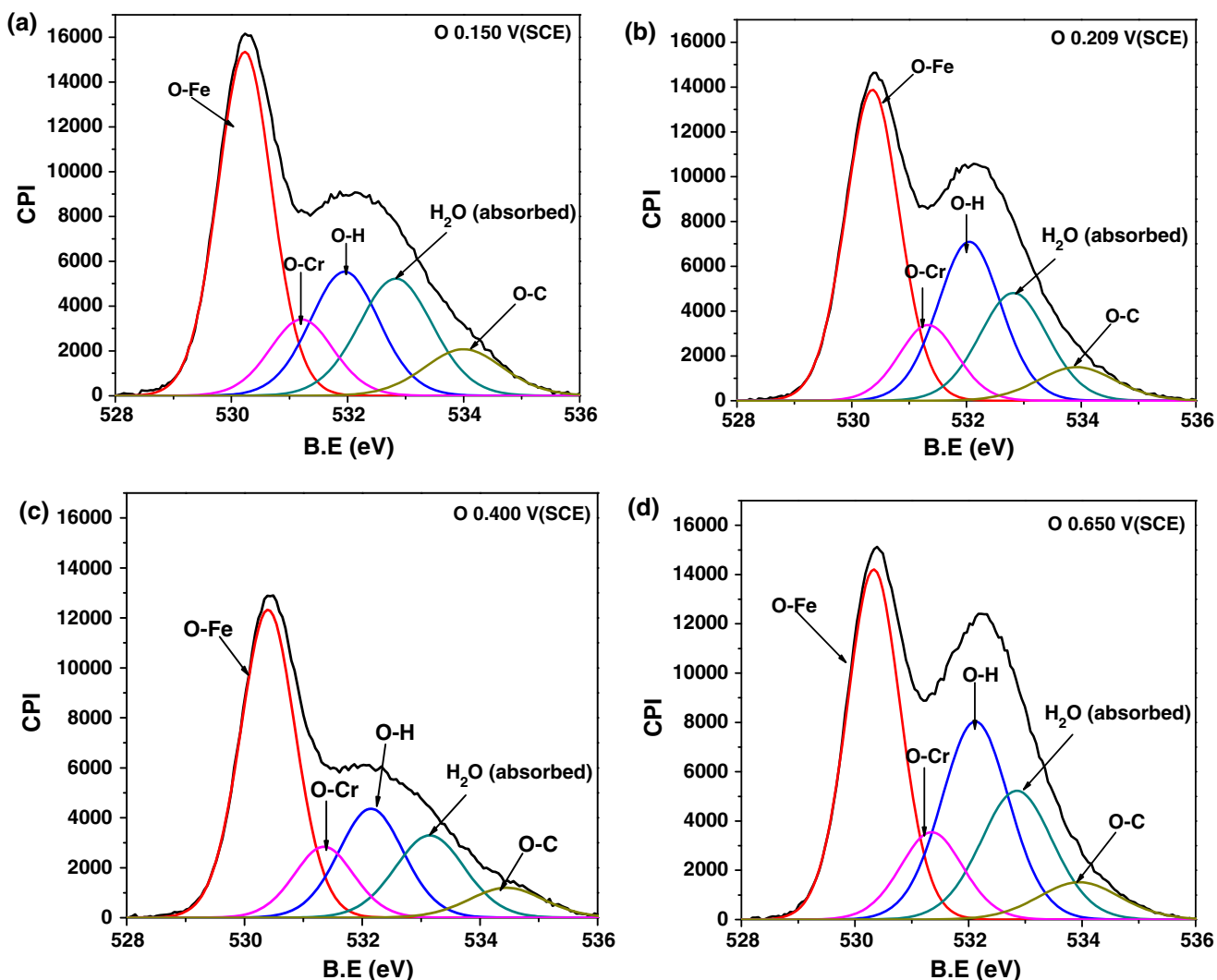


**Fig. 11** The XPS spectra showing oxygen peaks for potentiostatically polarized specimens at **a** 150 mV, **b** 209 mV, **c** 400 mV and **d** 650 mV(SCE) potentials

**Table 6** Elemental composition of passive film of modified 9Cr–1Mo at different potentials

Potential [mV(SCE)]	Cr (metallic) (%)	Cr (oxidic) (%)	Fe (metallic) (%)	Fe (oxidic) (%)
150	3.2	15.8	19.2	61.8
209	3.7	12.9	20.8	62.6
400	2.0	13.1	11.3	73.6
650	2.9	16.7	15.8	64.6

XPS analysis plots for Cr (2p) are shown in Fig. 10a–d. A well-defined metallic peak at  $\sim 574$  eV, a hydroxide (CrOOH) peak at  $\sim 577$  eV and a contribution from Cr<sub>2</sub>O<sub>3</sub> are seen in the Cr 2p spectra. The Cr 2p<sub>3/2</sub> spectrum shows a peak of Cr<sup>3+</sup> state at 576 eV [20] and a peak at 579 eV can be assigned to Cr<sup>6+</sup> [19]. Thus Cr was found to exist as Cr<sub>2</sub>O<sub>3</sub>, Cr(OH)<sub>3</sub> and CrO<sub>3</sub> at all the above potentials at which the specimens were passivated. The BE data for Cr 2p<sub>3/2</sub> compounds were obtained from literature and compared with the values obtained in our results and the peaks were assigned accordingly [25]. It was observed that Cr existed largely as Cr(III) in the form of different compounds like Cr<sub>2</sub>O<sub>3</sub>, CrCl<sub>3</sub>, Cr(OH)<sub>3</sub>; however, it was also found to exist as CrO<sub>3</sub> and Cr<sub>2</sub>O<sub>7</sub><sup>2-</sup> species. Although third Cr oxide peak was unexpected from a thermodynamic viewpoint it could be explained to be due to interacting processes from different elements in the steels and due to higher pH. It has been discussed by Clayton and Lu [26] and also Olsson [27] that CrO<sub>3</sub> can co-exist with Cr<sub>2</sub>O<sub>3</sub> in the inner oxide due to the similar standard free enthalpies they have. Although, Cr was detected in the form of Cr(VI) at all potentials, its intensity appeared to be the same in all the XPS plots, thus the ratio of Cr(III)/Cr(VI) could not be obtained. The B.E of Cr 2p<sub>3/2</sub> compounds obtained from this work and average data from literature are given in Table 5.

XPS analysis plots for O (1s) are shown in Fig. 11a–d. The O (1s) spectrum is composed of five peaks which correspond to the signals from oxygen in the iron oxide (O<sup>2-</sup>) at  $\sim 530.3$  eV, signals from oxygen in the chromium oxide (O<sup>2-</sup>) at  $\sim 531.3$  eV, oxygen in hydroxyl group (OH<sup>-</sup>) at  $\sim 532$  eV and chemisorbed water (H<sub>2</sub>O) at 532.9 eV. The B.E data for these peaks are correlated with the previous findings [28].

Estimation of the relative thicknesses of the passive films is done by comparing the relative intensities of the metallic contribution and the oxidic contribution of Fe and Cr on the surface to avoid any artifacts that might be caused by sputtering. The analysis showed that the order of increasing thickness of the passive film for the specimens was 209 mV < 150 mV < 650 mV < 400 mV(SCE) (Table 6). This could be explained from the potentiodynamic polarization curves for the respective specimens. The passive film formed at the potential of 150 mV started

to dissolve at 209 mV(SCE) resulting in thinning of the passive film and increase in the anodic current. The dissolution of Cr as Cr(VI), as discussed earlier, could be confirmed from the oxidic contribution of Cr (Table 6) at 209 mV(SCE), which is much lower compared to other potentials; the oxidic contribution of Cr was found to increase again at higher potentials. The contribution of Cr metal at higher potential was observed to decrease (Table 6), on account of pitting or transpassive potential. Beyond this potential, the passive film undergoes change in the chemical composition which has higher thickness, as is evident from XPS at 400 mV. From the polarization curve, 650 mV(SCE) falls in the transpassive/pitting region and hence the dissolution of the passive film results in thinning of the film; this is supported by the reduction of metallic contribution of Fe at these potentials. Also the relative concentration ratio of Cr to Fe is observed to be decreasing with increase in passive potential from 150 to 400 mV(SCE). But the maximum value was found to be for the specimen passivated at 650 mV(SCE). This can be explained based on the fact that the Fe oxides dissolve selectively in preference to Cr<sub>2</sub>O<sub>3</sub> oxide during transpassive dissolution/pitting corrosion, exposing the underlying Cr<sub>2</sub>O<sub>3</sub> to the medium. Thus it can be inferred that after the OCP is crossed, passive film becomes richer in Fe(III)/Cr(III) as discussed earlier.

#### 4 Conclusions

Based on the potentiodynamic anodic polarization experiments, optical microscopic, SEM observations and XPS analysis of the pitted specimens of modified 9Cr–1Mo–B, the following conclusions were drawn.

- (1) Chloride ions exerted a strong influence on the initiation as well as growth of pits in the lower concentrations of alkali; pit diameters as well as pit depths increased with increase in chloride ion concentration when added to 0.1 M sodium hydroxide solution.
- (2) At higher alkali concentration (0.2 and 0.5 M sodium hydroxide), pit depths and diameters decreased drastically. The increased pH did not favour the pitting

corrosion process by way of increasing the pH of the solution in the pit bottoms. Also, formation of soluble species like  $\text{HFeO}_2^-$  and  $\text{FeO}_2^{2-}$  on the surface destabilized the passive film, creating unfavourable conditions for pitting leading to shallow pits.

- (3) Apart from  $\text{M}_{23}\text{C}_6$  carbides/matrix interface, pits were also found to have initiated at the  $\text{Al}_2\text{O}_3$  inclusion/matrix interface.
- (4) XPS analysis of passive film showed the presence of  $\text{Fe}_3\text{O}_4$ ,  $\text{Fe}(\text{OH})_3$  at lower potentials (150 and 209 mV(SCE)) whereas  $\text{Fe}_2\text{O}_3$ ,  $\text{Fe}(\text{OH})_3$  and  $\text{FeO}_2^{2-}$  at higher potentials (400 and 650 mV(SCE)). At transpassive/pitting potentials Fe oxides dissolved selectively in preference to  $\text{Cr}_2\text{O}_3$  oxide, protecting the surface.
- (5) Based on the metallic and oxidic contributions, it was logically accepted that Fe existed as a hydroxide on top of  $\text{Cr}_2\text{O}_3$  and underent dissolution at transpassive/pitting potentials. Presence of Cr(VI) peak in the Cr spectra was justified because of the conducive pH conditions, which stabilized this species.

## References

1. Swaminathan S, Mallika C, Krishna N G, Thinaharan C, Jayakumar T, and Kamachi Mudali U, *Corros Sci* **79** (2014) 59.
2. Klueh R L, *Nucl Eng Des* **72** (1982) 329.
3. Kumar A, Choudhary B K, Laha K, Jayakumar T, Rao K B S, and Raj B, *Trans Indian Inst Met* **56** (2003) 483.
4. Thomas Paul V, Saroja S, and Vijayalakshmi M, *J Nucl Mater* **378** (2008) 273.
5. Pujar M G, Das C R, Thirunavukkarasu S, Kamachi Mudali U, Bhaduri A K, Brijitta J, and Tata B V R, *Mater Chem Phys* **130** (2011), 536.
6. Moreno D A, Molina B, Ranninger C, Montero F, and Izquierdo J, *Corrosion* **60** (2004) 573.
7. Abe F, Horiuchi T, Taneike M, in *Parsons 2003: Engineering Issues in Turbine Machinery, Power Plant and Renewables*, (eds) Strang A, Conroy R D, Banks W M, Blackler M, Leggett J, McColvin G M, Simpson S, Smit M, Starr F, Vanstone R W, The Institute of Materials, Minerals and Mining, London (2003), p 379.
8. Malik A U, Mayan Kutty P C, Siddiqi N A, Andijani I N, and Ahmed S, *Corros Sci* **33** (1992) 1809.
9. Mudali U K, Khatak H S, Dayal R K, and Gnanamoorthy J B, *J Mater Eng Perform* **2** (1993) 135.
10. Hoppe H W, Haupt S, and Strehblow H H. *Surf Interface Anal* **21** (1994) 514.
11. Pourbaix M., *Atlas of Electrochemical Equilibria in Aqueous Solutions*, NACE, Houston, TX (1974), p 308.
12. Ziemniak S E, *J Solut Chem* **21** (1992) 745.
13. Makar G L, and Tromans D, *Corrosion* **52** (1996) 250.
14. Sanchez-Amaya J M, Cottis R A, and Botana F J, *Corros Sci* **47** (2005) 3280.
15. Al-Mazeedi H A A, and Cottis, R A., *Electrochim Acta* **49** (2004) 2787.
16. Song W, Martin H J, Hicks A, Seely D, Walton C A, Lawrimore II W B, Wang P T, and Horstemeyer M F, *Corros Sci* **78** (2014) 353.
17. Chauveau E, Mantel M, and Nogueira R P, *Appl Surf Sci* **270** (2013) 90.
18. Grosvenor A P, Kobe B A, Biesinger M C, and McIntyre N S, *Surf Interface Anal* **36** (2004) 1564.
19. Macdonald D D, and Owen D, *J Electrochem Soc* **120** (1973) 317.
20. Asami K, and Hashimoto K, *Corros Sci* **17** (1977) 559.
21. Olsson C O A, Malmgren S, Gorgoi M, and Edström K, *Electrochim Solid-State Lett* **14** (2011) C1.
22. Olsson C O A, and Landolt D, *Electrochim Acta* **48** (2003) 1093.
23. Heine B, and Kirchheim R, *Corros Sci* **31** (1990) 533.
24. Fredriksson W, Depth profiling of the passive layer on stainless steel using photoelectron spectroscopy. Dissertation presented at Uppasala University, Angstromlaboratoriet, Lagerhyddsvagen, Uppasala (2012) p 59.
25. Biesinger M C, Brown C, Mycroft J R, Davidson R D, and McIntyre N S, *Surf Interface Anal* **36** (2004) 1550.
26. Clayton C R, and Lu Y C, *J Electrochem Soc* **133** (1986) 2465.
27. Olsson C O A, *Corros Sci* **37** (1995), 467.
28. Lin T-C, Seshadri G, and Kelber J A, *Appl Surf Sci* **119** (1997) 83.